Electron Injection Dynamics from Ru Polypyridyl Complexes to ZnO Nanocrystalline Thin Films

Neil A. Anderson, Xin Ai, and Tianquan Lian*

Department of Chemistry, Emory University, Atlanta, Georgia 30322

Received: July 28, 2003; In Final Form: October 10, 2003

Electron injection dynamics from $Ru(dcbpyH_2)_2(NCS)_2$ (RuN3) and $(Bu_4N)_2Ru(dcbpyH)_2(NCS)_2$ (N719) to nanocrystalline ZnO thin films were studied using transient IR spectroscopy. The injection dynamics using 400 nm excitation were found to be biphasic, consisting of a distinct <100 fs component (14−20%) and slower nonexponential rise that is fitted by a biexponential function with time constants of ∼20 ps and ∼200 ps. The fast component amplitude decreases to ∼5% at 530 nm excitation. Dye agglomeration was shown not to affect injection dynamics, although it reduced injection yield, suggesting the agglomerates do not contribute to electron injection within 1 ns. A two-state injection model, previously used to describe injection dynamics in TiO_2, was proposed for ZnO. The fast and the slow components were attributed to injection from unthermalized and relaxed excited states, respectively. Using this model, the injection time scales for these states were estimated to be 1.5 and 150 ps, respectively, both of which are an order of magnitude slower than corresponding rates to TiO_2. Possible reasons for the different injection dynamics in these semiconductors are discussed.

Introduction

Motivated by both applied and fundamental interests, electron transfer dynamics between molecular adsorbate and semiconductor nanoparticles have been intensely investigated for several years.[1−4] Understanding these processes is relevant to the design and improvement of Grätzel-type solar cells for which charge separation and recombination dynamics play a crucial role in determining the overall cell efficiency.[5,6] These systems also provide convenient media for studying ultrafast interfacial electron transfer, a poorly understood fundamental process that has relevance to many other semiconductor and metal nanomaterials-based devices.

Among many possible combinations of dye and semiconductor materials, solar cells based on $Ru(dcbpyH_2)_2(NCS)_2$ (abbreviated as RuN3, see Chart 1a, dcbpy = 4,4′-dicarboxy-2,2′-bipyridine)-sensitized TiO_2 nanocrystalline thin films have produced the highest solar-to-electric power conversion efficiency.[5,7] As the most heavily studied dye molecule, one method for achieving a more clear understanding of factors that control interfacial charge-transfer dynamics is to investigate injection dynamics from RuN3 to other semiconductors.[8−15] A particularly interesting comparison is between TiO_2 and ZnO. These semiconductors possess virtually identical band energetics,[4] but differ in their conduction band structure. The TiO_2 conduction band is comprised primarily of empty 3d orbitals from Ti^{4+},[16−18] while the ZnO conduction band is comprised primarily of empty s and p orbitals of Zn^{2+}.[17] They have very different densities of states and possibly different coupling with the adsorbate, both of which are expected to affect the electron injection rate.

It is generally well-accepted that photoinduced electron injection from RuN3 to TiO_2 proceeds with a sizable <100 fs ultrafast component, in addition to other slower components.[8,19−34]

CHART 1: Schematic Structure of (a) RuN3 on ZnO and (a)ReC0A

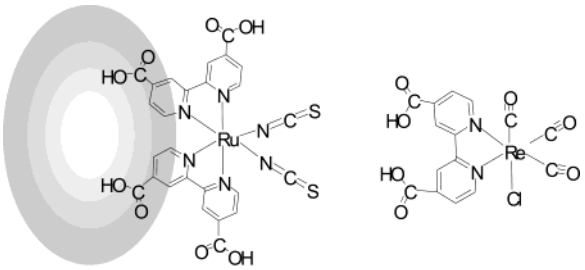

a b

The biphasic injection kinetics are attributed to competition between ultrafast electron injection from the initially populated ^{1}MLCT excited state and rapid intramolecular relaxation.[8,30−33] The fast component corresponds to injection from the unthermalized electronically excited state, while slow components correspond to injection from relaxed ^{3}MLCT states near the band edge. The relative amplitude and rate of the slow component was found to depend on the excitation wavelength, solvent, and pH and cation concentration at the interface.[21,28,31−34]

Although parallel work has been done to experimentally characterize electron injection to ZnO, some confusion has arisen regarding the rate of photoinduced electron transfer from RuN3 and related N719 $[(Bu_4N)_2Ru(dcbpyH)_2(NCS)_2]$. Our group previously observed multiexponential injection with a small <100 fs injection component, and multiple slower components with time constants ranging to hundreds of picoseconds, more than an order of magnitude slower than injection from RuN3 to TiO_2.[9] Subsequently, Bauer et al. argued for sub-300 fs injection from N719 on the basis of a fast observed rise in the visible transient absorption at 770 nm that was attributed to electron injection.[10] However, a detailed transient absorption study of RuN3 on TiO_2 showed that this wavelength lies very close to an isosbestic point between the reactant RuN3* and

* Author to whom correspondence should be addressed. E-mail: tlian@emory.edu.

10.1021/jp036201h CCC: $25.00
Published on Web 12/02/2003

product $RuN3^+$ absorption bands.[32,33] As N719 and RuN3 have identical chromophores, the same should be true for N719. Therefore, an instantaneous rise at 770 nm will be observed regardless of injection rate. The rise time probed at this wavelength alone cannot reliably indicate electron injection dynamics. In a more recent study of RuN3/ZnO by Furube and co-workers,[11] time-resolved spectra in the visible and near-IR were recorded. The result corroborated slow electron injection into bulk ZnO, but it also noted a rapidly formed broad near-IR absorption band that disappeared as electrons were injected into ZnO. The origin of the band was not unambiguously determined, but exciplexes between RuN3 and ZnO were suggested possible candidates. Further clarification of the injection to ZnO is necessary to resolve uncertainties and better understand the factors influencing electron transfer to semiconductors.

The present work utilizes ultrafast IR spectroscopy to investigate the injection rate from molecular adsorbates into nanoporous ZnO film. This technique allows simultaneous and separable detection of signals arising from the dye molecules and from the injected electrons. As a result, the electron injection rate can be clearly determined. We investigate several factors that may influence injection rate. Among the varied factors are sensitization conditions (degree of dye agglomeration), excitation power, excitation wavelength, and dye structure. Investigation of the injection rate as a function of these conditions will assist in understanding factors controlling the electron injection rate to ZnO, thus clarifying the injection mechanism.

Experimental Section

Sample Preparation. ZnO nanoparticle colloids were prepared similarly to a published procedure.[35] Briefly, 10 mmol of $Zn(Ac)_2$ (Aldrich) was added to 5 mL of absolute ethanol and cooled to 0 °C. Separately, 14 mmol of $LiOH{\cdot}H_2O$ was dissolved in 95 mL of ethanol at room temperature, cooled to 0 °C, and slowly added to the Zn(II) solution under vigorous stirring. The mixture was thoroughly washed with ~250 mL of hexane and centrifuged to remove the supernatant liquid. The ZnO precipitant was dissolved in ethanol to make a ZnO colloid and was washed with hexane twice more. The colloid was applied to polished sapphire windows to form a thin film, which was dried in air, then baked at 400 °C for 1 h. Preparation of TiO_2 and ZrO_2 films have been described previously.[7,8]

RuN3 and N719 were used as received from Solaronix (Lausanne, Switzerland). The synthesis of $Re(CO)_3Cl(dcbpy)$ (ReC0A, see Chart 1b) was previously described in detail.[36,37] Sensitization of the nanoporous semiconductor films was performed by soaking the films in a dye solution. Optical densities of the sensitized films were controlled by varying the dye concentration and sensitization time. ReC0A-sensitized ZnO was prepared by soaking the film in a 2 g/L methanolic solution of the dye for 30 min. For RuN3-sensitized ZnO, films were typically soaked in 1 mg/mL ethanolic solutions of RuN3 for 2−4 h to obtain an optical density of 0.2−0.3 at 400 nm, except as noted. All sensitized films are allowed to dry by exposure to air prior to measurements.

Ultrafast Infrared Transient Absorption Measurements. The tunable infrared spectrometer used for these studies utilizes a 1 kHz regeneratively amplified Ti:sapphire laser system (800 nm, 100 fs, 900 μJ/pulse). Difference frequency generation from the signal and idler of an IR OPA produced the tunable mid-IR probe pulses, which had a ~250 cm^{-1} bandwidth. Frequency doubling the laser fundamental provided the 400 nm pump beam. Details of the experimental setup have been previously reported.[38,39]

Except when otherwise noted, experiments were performed using a pump beam of 2 μJ/pulse at 400 nm. The pump beam had a spot size of 500 μm at the sample, while the mid-IR probe beam was focused to 300 μm at the sample. The probe was dispersed in a spectrometer, and detected using a 32-element MCT array detector. The spectral resolution was 15 nm (~6 cm^{-1} at 2100 cm^{-1}). Zero time delay was defined and the instrument response was characterized utilizing a CdS film, which gives an instantaneous mid-IR absorption response to the pump beam. Typically, the instrument response at the sample was well characterized by a 200−250 fs fwhm Gaussian function. During data collection, samples (exposed to air) were constantly translated in order to avoid accumulation of permanent photoproducts.

Results

Correlation of Dye Vibrational Spectrum with Injected Electron. The pump power dependence of signal from RuN3/ZnO was tested in order to ensure that subsequently obtained signals result from single photon excitation of RuN3. Figure 1 shows kinetic traces for RuN3/ZnO probing at 2010 cm^{-1} using three different 400 nm excitation powers (0.9 μJ/pulse, 2.2 μJ/pulse, 5.5 μJ/pulse). Since this probe wavelength is largely free of significant contribution from the dye vibrational modes, the signal arises from the broad mid-IR absorption of electrons injected to ZnO. All three traces exhibit very similar dynamics. Within error, the signal size normalization factors (2.2, 1, 0.5) correspond linearly to differences in pump power. The results clearly indicate that the observed injection arises from single-photon excitation of the dye. Falling well within the linear regime, all following results were obtained using ~2 μJ pump power.

The mid-IR data presented above and previously[9] relied solely on the broad ZnO injected electron dynamics as a probe of electron transfer. The electron absorption signal depends on both the population dynamics and absorption cross-section change. If the latter is small, the measured electron signal can be used to directly monitor the injection dynamics. However, cross section decay can sometimes occur on the <1 ns time scale due to electron energy relaxation.[31,39,40] For adsorbates with strong vibrational bands, transient mid-IR spectroscopy affords the opportunity to simultaneously study the adsorbate vibrational spectrum and the broad absorption of injected electrons in the semiconductor, allowing the measurement of both the injection

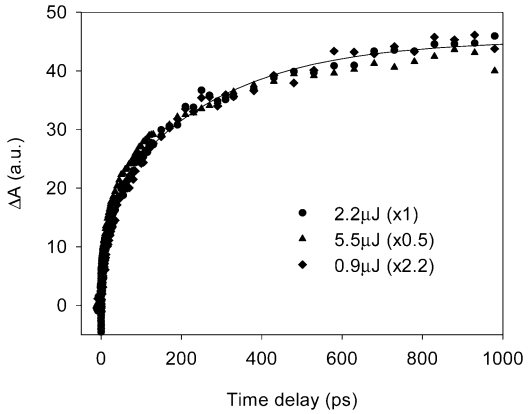

Figure 1. Normalized kinetic traces of RuN3/ZnO probing at 2010 cm^{-1} and using three different 400 nm excitation powers, as indicated on the figure. ZnO naked film signal has been subtracted to give the displayed traces. The size-normalization scale factors (inside the parentheses of legend) used to obtain the plot correspond, indicating a linear dependence of signal size on pump power.

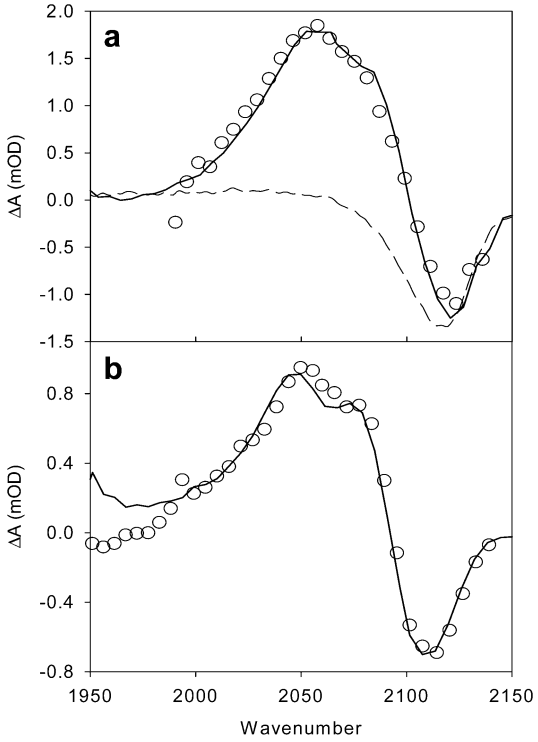

Figure 2. (a) Difference spectra of RuN3/ZrO_2 10 ps (solid line) and RuN3/ZnO 2 ps (open circles). The inverted and scaled RuN3/ZnO static FTIR spectrum is shown as the dashed line. (b) Difference spectra of N719/ZrO_2 10 ps (solid line) and N719/ZnO 2 ps (open circles). All samples show photobleaching of the ground-state CN stretch and a red-shifted absorption band. The ZrO_2 and ZnO difference spectra at these time delays are virtually identical.

kinetics and electron cross-section decay. Here, we attempt to correlate adsorbate vibrational spectra with the ZnO injected electron signal.

Ground-state RuN3 exhibits an absorption peak from the CN stretching band at ~2114 cm^{-1}, containing both the symmetric and antisymmetric CN stretching modes. Figure 2 shows difference spectra from RuN3 and N719 on ZrO_2 at 10 ps, with the inverted and normalized RuN3/ZnO static FTIR spectrum shown for reference. Both of the transient spectra exhibit bleach peaks from the ground-state CN stretch, and red-shifted absorption bands. No broad underlying absorption attributable to electrons injected to the semiconductor was observed for either RuN3 or N719/ZrO_2 at any time delay. Furthermore, the absorption peak observed here is ~2050 cm^{-1}, whereas reference 41 shows the CN stretching peak of oxidized RuN3 to be at ~2025 cm^{-1}. These results indicate that charge injection does not occur from either sensitizer to ZrO_2, consistent with the energetic unfavorability of transfer.[27,29] The observed difference spectra are therefore attributable to the sensitizer excited state. The CN stretch red-shifts in the MLCT excited state, suggesting a weakening of the CN bond. This is consistent with a recent DFT calculation, which shows that the HOMO contains a significant contribution of the NCS group in addition to Ru d orbitals, while the LUMO is mostly bipyridine π^* orbitals.[42] Further shift is seen for the oxidized form due to additional decrease of the charge density on Ru, consistent with the difference spectrum attributable to oxidized RuN3.[41]

To compare the difference spectra attributable to the sensitizers on ZnO at 2 ps, it is necessary to subtract the signal attributable to injected electrons. At this time delay, the electron signal is ~20% of its value at 1 ns. To accurately subtract the electron signal, the spectrum of electrons injected into ZnO was

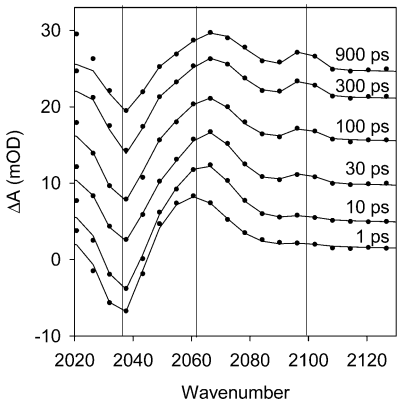

Figure 3. Transient spectra for ReC0A/ZnO at the indicated time delays. The bleach of the highest-energy CO stretch in the electronic ground state is seen at 2035 cm^{-1}. An absorption peak attributable to the molecule in the electronic excited state is present at ~2063 cm^{-1}. The oxidized ReC0A peak is seen at 2096 cm^{-1}. Underlying the ReC0A modes is a broad absorption signal, attributable to injected electrons in the semiconductor. Both the oxidized peak and the electron signal grow with time, as the excited state decays.

determined using coumarin-343/ZnO as a reference. Since coumarin-343 exhibits no strong vibrational modes in this region, the obtained spectrum is attributed solely to the injected ZnO electron, and was scaled for subtraction.[43] The resulting subtracted RuN3 and N719/ZnO spectra at 2 ps closely resemble the corresponding ZrO_2 spectra, also exhibiting the narrower bleach peak and higher energy absorption band. This provides direct evidence that for RuN3 and N719/ZnO at 2 ps, most photoexcited molecules have not undergone electron injection, supported by the relatively small electron signal at this time delay. Quantitative correlation between electron dynamics and evolution of the adsorbate vibrational spectrum could not be tested for RuN3/ZnO because of the much larger extinction coefficient of the electron absorption signal. As injection proceeds, the relative contribution of the RuN3 difference spectrum becomes too small to clearly resolve above the underlying electron absorption. Nevertheless, a red-shifted absorption band was observed for N719/ZnO at 300 ps, indicating qualitative correspondence between injected electron and adsorbate signals.

To achieve quantitative correlation between adsorbate and ZnO electron signals, we also studied ReC0A on ZnO. This dye was selected because it retains structural similarity to RuN3, with a central metal and bipyridene ligand that binds to the semiconductor through carboxylate groups. ReC0A has three CO ligands, with large absorption cross-sections for the stretching modes. As a result, they are easily observed, even without subtracting the ZnO injected electron signal.[38,44] Furthermore, the peaks attributable to excited state and oxidized dyes are narrower and better resolved than for RuN3 or N719. The time-evolution of the ReC0A/ZnO difference spectrum in the region of the highest-energy CO stretch is shown in Figure 3. Peak positions for the CO stretch in the electronic ground, excited, and oxidized states were previously assigned.[36] The bleach signal at 2035 cm^{-1} corresponds to the frequency of the CO stretch in the ReC0A electronic ground state. This band does not show significant decay within 1 ns, although clear analysis is complicated by overlap with other bands. An absorption peak is seen at ~2063 cm^{-1}, shifting to higher energy within the first 10 ps. This peak corresponds to the CO stretch for the electronically excited ReC0A. Its blue-shift at early time is attributed to vibrational relaxation dynamics of the adsorbate excited state and has been observed previously for the same molecule on ZrO_2.[38] It is strongest at early delays, gradually

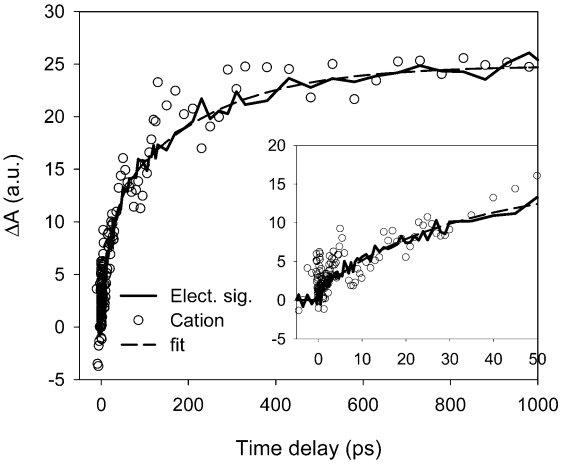

Figure 4. The solid line represents the electron signal in ReC0A/ZnO, probed at 2130 cm^{-1}. The electron signal fit is shown as the dashed line. The open circles correspond to the integrated intensity of the oxidized ReC0A CO stretching peak, calculated at each time delay. Signals are normalized for clear comparison. The inset shows the early-time dynamics of both signals. The injected electron and oxidized dye signal dynamics correspond at all time delays, indicating that either may be used to track electron injection.

decaying with time, but retains significant intensity, even at 900 ps delay. Correspondent with the excited-state decay is the growth of an absorption band at 2096 cm^{-1}, arising from the oxidized ReC0A resulting from electron injection.

Figure 4 compares the dynamics of the broad injected electron signal probed at 2130 cm^{-1} with the intensity of the ReC0A oxidized peak. The electron signal was fit using a three-exponential rise convoluted with the instrument response function. The time scales (relative amplitudes) were subpicosecond (4%), 23 ps (38%), and 220 ps (58%). The oxidized peak trace was obtained by integrating the area of the oxidized peak at each time delay. As a result of the comparatively small absorption peak, this trace is relatively noisy. Nevertheless, it reproduces the injected electron signal within error at all time delays, demonstrating that either signal may be used to track electron injection. Since the injected electron signal is more easily resolved and less noisy than the adsorbate signals, further results will utilize it to determine electron-transfer dynamics.

Investigation of Factors Influencing Injection Rate and Yield. Figure 5 shows the effect of excitation wavelength on RuN3/ZnO charge injection. The same sample was excited at 400 and 530 nm. The signals are size-normalized for comparison due to significant uncertainty in relative excitation densities for the two wavelengths. The ZnO naked film signal at 400 nm is also shown, and has already been subtracted to give the displayed RuN3/ZnO trace. Negligible naked film signal was obtained using 530 nm excitation. Comparing the excitation wavelengths, the clearest difference is the substantial reduction of the fast injection component exciting at 530 nm relative to 400 nm. Both traces were fit by convoluting a three-exponential rise with the Gaussian instrument response determined from measurement of CdS film. Fitting the 400 nm trace yielded time constants (relative amplitude) of <100 fs (14%), 20 ps (31%), and 230 ps (55%). Testing a number of samples, the amplitude of the fast component ranged from 14 to 20%, consistent with our previous report.[9] For 530 nm excitation, the subpicosecond component dropped to ∼5%, while the fitting parameters for the slow components were 20 ps (43%) and 220 ps (51%), similar to those obtained at 400 nm. The slow components can be described by multiple-exponential, stretched exponential, or Gaussian distribution of exponential functions. We use biexponential functions to fit the slow components because they are the minimum number of exponentials needed to achieve a satisfactory fit, not to imply a physical model. Furthermore, the injection signal continues to grow at 1 ns, suggesting that there are likely even slower injection components. In fact, Bedja and co-workers measured the injection time of $[Ru(II)(bpy)_2(dcbpy)]^{2+}$-sensitized ZnO thin film in the nanosecond time scale by microwave absorption and found injection times of 9.6 and 83 ns.[45] Incomplete injection at 1 ns is clearly shown for ReC0A/ZnO (Figure 3), which exhibits a significant (∼50%) excited population remaining at 900 ps.

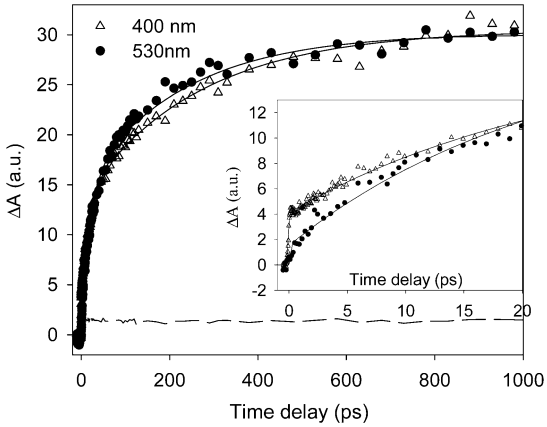

Figure 5. Normalized electron injection traces for RuN3/ZnO exciting at 400 nm (triangles) and 530 nm (circles). The dashed line is the ZnO naked film signal at 400 nm, which has already been subtracted from the N3/ZnO trace. The inset shows the early time dynamics. The primary difference between the signals is the ∼14% fast injection component exciting at 400 nm, dropping to ∼5% exciting at 530 nm. Subsequent dynamics are similar.

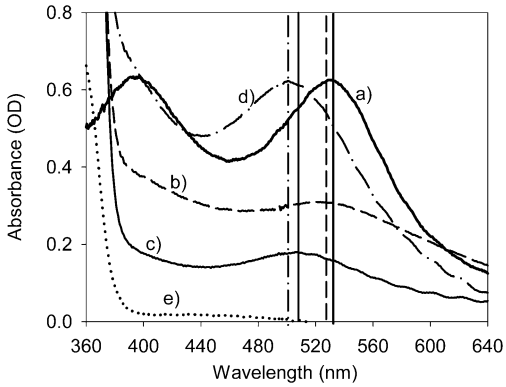

Figure 6. Static absorption spectra for agglomeration-dependent samples. RuN3/TiO_2 (a, thick solid line) has the farthest red absorption maximum at 530 nm, followed by N719/ZnO (b, dashed line) at 525 nm, low-loading RuN3/ZnO (c, thin solid line) at 506 nm, and high-loading RuN3/ZnO (d, dot−dash line) at 500 nm. Peak wavelengths for each sample are indicated by the vertical lines with corresponding line styles. The naked ZnO film spectrum is shown as the dotted line.

To explore the possibility that the slow injection components are caused by the formation of agglomerates, three samples were prepared: (1) low-loading RuN3/ZnO (ZnO sensitized in RuN3 1 mg/mL solution for 2 h), (2) high-loading RuN3/ZnO (ZnO sensitized in RuN3 1 mg/mL solution for 12 h), (3) ZnO sensitized in N719 solution (2.5 mg/mL, sensitized 12 h). The static absorption spectra for these samples are shown in Figure 6. The position of the absorption peak shifts between the samples, appearing at 500 nm in sample (1), 506 nm in sample (2), and 525 nm in sample (3). The RuN3-sensitized films are substantially blue-shifted relative to the 530 nm peak for RuN3/

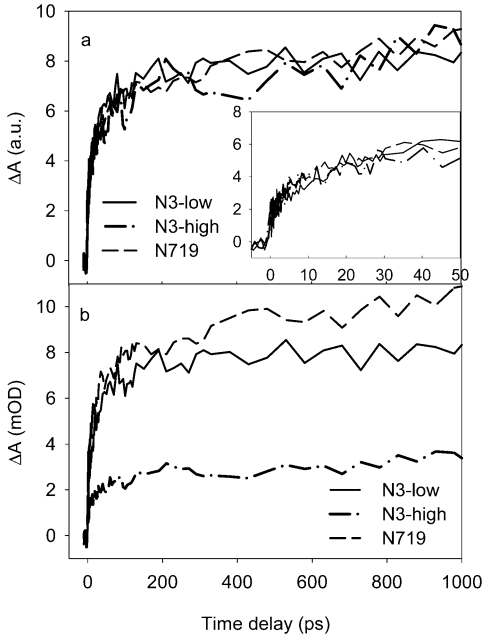

Figure 7. (a) Size-normalized injected electron traces for N719/ZnO (dashed line), low-loading RuN3/ZnO (solid line), and high-loading RuN3/ZnO (dashed−dot line). The inset shows the early time dynamics. All traces are identical within error. (b) The same traces, normalized by their absorbance at 400 nm to show relative yield. N719/ZnO has the highest injection yield, ∼3 times higher than high-loading RuN3/ZnO. Naked film signals have been subtracted in all cases.

TiO_2, while the N719/ZnO nearly corresponds with the 527 nm solution peak.

Injected electron kinetic traces exciting at 400 nm for the three samples are shown in Figure 7. The small ZnO naked film signal has already been subtracted from each to give the displayed traces. The traces correspond to the same excitation power and pump−probe overlap, and have been corrected by differences in sample optical density at 400 nm. This correction produces signal intensities that indicate the relative injection quantum yield. At 1 ns time delay, the relative yield for the N719 sample is ∼25% greater than for the low-loading RuN3 sample, and ∼300% greater than the high-loading RuN3 sample. Despite the large variation in yield, the size-normalized signals all exhibited virtually identical injection dynamics.

Discussion

Origin of Slow Electron Transfer to ZnO. We have shown that the rise of injected electron absorption in RuN3/ZnO and N719/ZnO is multiexponential and dominated by slow components with time constants up to and perhaps longer than hundreds of picoseconds. The adsorbate vibrational spectrum also indicates that at 2 ps, the spectrum is dominated by adsorbate excited states, with negligible contribution from oxidized molecules. Quantitative dynamics correlation between electron signal and oxidized adsorbate peak was demonstrated using ReC0A/ZnO.

The observation of multiexponential injection with time scales extending to hundreds of picoseconds is qualitatively consistent with earlier findings by our group for RuN3/ZnO.[9] Small quantitative differences between the two studies appear to correlate with use of different batches of ZnO prepared at different times. This sensitivity to sample is reasonable considering that the adsorbate excited-state potential (−0.85 V vs SCE[34,46]) is near the band edge of ZnO. The conduction band edge of ZnO is −0.66 V at pH = 7 and exhibits a Nernstian shift of −60 meV per increased pH unit.[4,47] The proton concentration on a dry film (exposed to air) is not known and we suspect that the band edge is substantially more negative than −0.66 V. The density of electron-accepting states in ZnO within this energy range varies rapidly with energy and depends sensitively on trap state density. As a result, the electron injection rate can be sensitive to sample conditions. This phenomenon was also observed for Ru dyes on TiO_2, in which the slow components, due to injection from relaxed excited state near the band edge, was found to vary among reports of different groups[20,21,28,31−34] and shown to be dependent on sample conditions(solvent, pH, and excitation wavelength).[31] Work is underway to more systematically investigate which aspects of the colloid or the films may affect the injection rate. Nevertheless, injection from RuN3 to ZnO is clearly much slower than the corresponding injection to TiO_2, despite the similarities in semiconductor energetics.[4]

A recent study of RuN3/ZnO showed a rapidly formed near-IR transient absorption species (600−1400 nm) that was not assignable to known dye-excited states or to injected electrons.[11] Decay of this absorption feature was correlated with growth of the injected electron signal at 2 μm, and was also in agreement with the injection we previously reported, probing in the mid-IR.[9] The intermediate was assigned to a neutral or ionic exciplex formed between the dye excited state and ZnO.[11] The present results clearly show that for RuN3 on ZnO, the transient IR absorption spectrum at 2 ps corresponds to RuN3*. For ReC0A/ZnO, the growth of the oxidized adsorbate and injected electron population are concomitant and also correlated with decay of the ReC0A excited state. For both systems, we do not observe any intermediate species other than the adsorbate excited state. As a result, it seems highly unlikely that the new near-IR band is due to an ionic exciplex, as this would imply that the intermediate species should have an IR spectrum that is closer to the oxidized form than to the neutral excited state. A neutral exciplex may be consistent with our observation, as it would rationalize the observation of dye excited-state-like vibrational spectrum of absorbates in the mid-IR transient spectra prior to charge injection.

In explaining the slow observed injection to ZnO, the possible contribution of agglomerates to the slow injection dynamics was proposed previously[10] and must be considered. RuN3/ZnO cells are known to exhibit decreased quantum efficiency at higher dye loading (i.e., longer sensitizing times).[10,48,49] This appears to be correlated with formation of large agglomerate particles, likely due to dissolution of surface Zn^{2+} facilitated by low local pH at the surface arising from solution conditions or acidic protons on the sensitizer.[50] The dissolved ions complex with the dye molecules and agglomerate in the pores and on the surface of the ZnO as nano- and microcrystals, substantially reducing the cell efficiency.[12,48,49]

Agglomeration effects on the observed injection dynamics were studied using ZnO films sensitized with N719 and high and low concentrations of RuN3. The N719 dye was selected because it is a doubly deprotonated version of RuN3. Containing fewer acidic protons, it may exhibit less agglomeration tendency than RuN3.[10,48] The degree of agglomeration may be qualitatively observed using the absorption spectra of the samples. The absorption and fluorescence spectra of these complexes are known to be sensitive to the binding environment.[49,51] A significant blue-shift of the RuN3 535 nm absorption band has been observed in samples with higher concentration (greater agglomeration).[9,10] This is also shown in Figure 6, where the N719/ZnO spectrum peak nearly matches the solution wave-

length. The low-loading RuN3/ZnO spectrum is blue-shifted, and the high-loading RuN3/ZnO spectrum shows a greater blue-shift. This result is qualitatively consistent with the anticipated agglomeration characteristics.

Injection results presented in Figure 7 clearly indicate that the observed slow injection into ZnO is not significantly correlated with agglomerate formation. The normalized signals for all three samples are virtually identical. It should be noted that the insensitivity of dynamics to film loading was also demonstrated previously, although all the lowest concentration studied was greater than any of the samples presented here.[9] Although it appears not to modify injection dynamics within 1 ns, agglomeration clearly affects the injection yield. N719/ZnO produced the highest quantum yield for injection, three times larger than the high-loading RuN3/ZnO sample. The relatively high N719 yield is consistent with the report that ZnO solar cell performance was improved using N719 rather than RuN3 as the sensitizer.[10]

The observed slow injection does not arise from diffusion processes in agglomerates. Rather, differences in yield due to agglomeration are caused by the inability of photoexcited agglomerate particles to inject electrons to ZnO on the <1 ns time scale. Agglomerate particles have been shown to grow quite large, filling the ZnO pores and accumulating on the surface.[49,52] As a result, most agglomerate excitations are localized far from the ZnO interface, and it is unlikely that they will diffuse there prior to decay. This assessment is further supported by the linear dependence of the injection signal to pump power (Figure 1). Increasing the excitation density results in a higher number of excitations in each agglomerate particle, increasing the possibility for quenching between excited-state molecules. It was shown previously under high excitation power that quenching can happen in nanocrystalline thin films sensitized by similar dyes.[38] This should affect the injection rate or yield if agglomerates can also inject electrons on the <1 ns time scale. The lack of any significant change in injection yield or dynamics indicates that excitations resulting in injection are isolated, likely coming from dye molecules at the ZnO interface rather than diffusion through agglomerate particles.

Comparing Electron Injection in ZnO and TiO_2. Having established that agglomerate formation is not responsible for the slow injection to ZnO, the large difference in injection rate between the semiconductors merits further examination. Electron injection from RuN3 to either ZnO or TiO_2 shows biphasic kinetics, with the former composite dominated by slow components and the latter by fast components.[8,19−34] Extensive studies of RuN3 on TiO_2 have shown that biphasic kinetics are caused by competition between ultrafast electron injection from the initially populated ^{1}MLCT excited state and rapid intramolecular relaxation.[21,28,31−34] The fast component corresponds to injection from unthermalized electronically excited states and slow components correspond to injection from relaxed ^{3}MLCT states near the band edge. If these two components are attributable to electron injection from different excited states, it is appropriate to compare the fast and slow injection components separately. We have proposed a two-state injection model to explain the biphasic injection kinetics in RuN3 on TiO_2.[31] It also accounts for the observed dependence of injection kinetics on excitation wavelength, solvent, and pH and cation concentration at the interface.[21,28,31−34] We propose that the biphasic injection kinetics on ZnO can also be described by the same two-state injection model, shown in Scheme 1.

According to the model, photoexcitation of the dye immediately produces an unthermalized ^{1}MLCT excited state. This

SCHEME 1: Two-State Injection Model

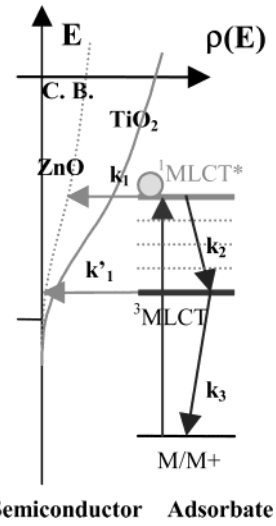

state can either inject electrons directly to the semiconductor (rate k_1) or undergo vibrational relaxation and intersystem crossing (ISC) to the thermalized ^{3}MLCT excited state (rate k_2). This state also injects electrons to the semiconductor (rate k_1'). For the present experiments, injection is the only decay mechanism for the relaxed excited state, as the excited-state lifetime of RuN3 (in solution or adsorbed on noninjecting substrate) is much longer than the 1 ns window studied here.[7,28] Assuming $k_1 \gg k_1'$, the electron population in the semiconductor is given by eq 1

$$N_e(t) = N_0\left[\frac{k_1}{k_1+k_2}(1-e^{-(k_1+k_2)t}) + \frac{k_2}{k_1+k_2}(1-e^{-k_1't})\right] \quad (1)$$

where the first term is injection from the unthermalized excited state, and the second term is injection from the relaxed excited state.[31]

In eq 1, N_0 is the total number of excited molecules that are able to undergo electron transfer. Noninjecting excited molecules, such as the agglomerates in RuN3/ZnO, are not included. Branching between hot excited-state injection and dye relaxation is therefore controlled by the ratio $k_1/(k_1 + k_2)$. Despite the obvious simplifications inherent in the model, it has been successfully used to obtain a more clear understanding of factors influencing electron injection.[28,31]

The qualitative predictions of the two-state model are supported by comparing the 400 and 530 nm excitation traces. At 530 nm excitation, the injection kinetics contains ∼5% fast component. Exciting at 400 nm results in a higher-energy hot excited state, which is expected to have a faster k_1 due to higher density of conduction band states. It may also slow k_2, as there is more excess energy to dissipate. Within the model, both of these effects may be expected to increase the fast injection component. The slower injection components are largely unchanged, as they correspond to injection from the relaxed excited state, which is independent of excitation wavelength. This was seen in the data where reduced fast injection was obtained exciting at 530 nm compared with 400 nm, while the slower injection components were similar for both excitation wavelengths.

For RuN3 excited at 530 nm, $k_2 \approx (75\text{ fs})^{-1}$.[28,32,33] The rate k_1 may therefore be estimated for RuN3/ZnO excited at 530 nm. Based on the 5% fast injection yield in the fit, $k_1 \approx (1.5\text{ ps})^{-1}$. For RuN3/$TiO_2$, the amount of fast injection at 530 nm excitation is ∼35%−60%, resulting in $k_1 \approx (50-140\text{ fs})^{-1}$.[23,31,33]

Quantitative determination of k_1 for 400 nm excitation is not possible because k_2 is not known in this case. However, comparison between k_1 on ZnO and TiO_2 is possible, since it may be reasonable to assume that k_2 is largely semiconductor-independent. In RuN3/TiO_2, the fast rise accounted for ~60−80% of the injection.[31,33] Compared with the ~14−20% observed here, this gives a ~7−20 times faster k_1 for TiO_2 than ZnO, similar to the ratio shown above for 530 nm excitation. The slow injection component is nonexponential in both TiO_2 and ZnO. The average time constant is 150 ps in ZnO and ~9−20 ps for TiO_2 films under different conditions.[23,31,33] Therefore, injection from the relaxed state to TiO_2 is about 7−16 times faster than to ZnO.

It should be noted that the relative amount and the rate of slow injection components in RuN3/TiO_2 vary in different reports and depend on sample condition.[23,31,33,34] Similar variation is also observed for RuN3/ZnO. For RuN3 on dry TiO_2 and ZnO, the electron-accepting states for the slow components are near or below the band edge and their density is sensitive to sample condition. The amount of fast component reported here for ZnO should be considered only as an upper limit, since injection appears to be incomplete at 1 ns. If > 1 ns injection components are included, the fast component amplitude is smaller and the average rate of slow component is even slower, which would increase the ratio of injection rate between TiO_2 and ZnO. These uncertainties introduce significant error in our quantitative estimate of the relative injection rate to TiO_2 and ZnO. Nevertheless, electron injection from RuN3 to TiO_2 appears to be at least an order of magnitude faster than to ZnO.

According to Marcus theory of interfacial electron transfer, slower injection to ZnO than TiO_2 may be caused by differences in electronic coupling strength and density of semiconductor states.[53,54] The TiO_2 conduction band is comprised primarily of empty 3d orbitals from Ti^{4+},[16−18] while the ZnO conduction band is comprised primarily of empty s and p orbitals of Zn^{2+}.[17] One effect of the differing band structures is a higher density of states in the TiO_2 conduction band. From the effective mass of the conduction band electron in TiO_2 (5−10 m_e) and ZnO (0.3 m_e),[47,55] the density of states near the conduction band edge is predicted to be as much as 2 orders of magnitude higher in TiO_2.[47] However, for states high above the band edge, (likely the accepting states for fast injection), the simple estimate of density of states from effective mass may no longer be valid. In addition to the differences in state density, another factor that may influence electron-transfer dynamics is differences in the electronic coupling between the dye-excited state (donor) and semiconductor conduction band (acceptor). It has been argued that the π symmetry T_{2g} d orbitals of Ti^{4+} may have better overlap with the dye π^* orbitals.[9,56]

Some recent theoretical studies have sought to incorporate these effects for prediction of injection rates for ZnO relative to TiO_2.[56,57] Using periodic hybrid ab initio Hartree−Fock density functional theory, the electronic interactions between isonicotinic acid and ZnO and TiO_2 surfaces were calculated.[57] Similar width of the adsorbate LUMO was found, from which electron injection time of 1−100 fs was estimated for both systems. However, the LUMO level was found to be at 2.4 V higher than the conduction band edge. This calculation may be relevant to electron injection from the initially prepared Franck−Condon state in our RuN3 study, which is estimated to be about 2 V higher than the conduction band edge. It is unlikely to accurately account for injection from the relaxed excited state, which is near or possibly below the band edge.

In a study using a one-dimensional tight-binding model, it was predicted that injection to ZnO would be a few times slower than to TiO_2, but that both would fall within the femtosecond domain at states above the band edge.[56] It is also notable that the calculated rates drop rapidly as the injecting state approaches band edge. While this very simplified model is not expected to quantitatively explain the experimental result, it does show that injection rate depends sensitively on the energetics of the adsorbate when it is near the conduction band edge.

There is some indication that the theoretical predictions may have more validity higher above the band edge, as evidenced by faster injection to ZnO for organic dyes with higher-lying excited states,[58,59] as well as our estimated 1.5 ps injection time from the hot excited state of RuN3. It appears that to fully understand the observed injection rate differences in TiO_2 and ZnO, adsorbates with energy ranging from near to high above the conduction band edge should be investigated both experimentally and theoretically. Theoretical methods that can accurately calculate adsorbate energetics, density of states in semiconductor, and electronic coupling strength are needed. Furthermore, an accurate description of the RuN3/ZnO system, in which slow injection to states near the band edge is dominating, may require a more realistic description of defect states. These states have been shown to play a significant role in electron-transfer processes when the adsorbate potential is near or below the band edge.[15,40,60,61] A recent study comparing back electron-transfer dynamics in dye-sensitized ZnO and TiO_2 have shown significant trap-state densities in both films.[62]

Conclusions

Electron injection kinetics from RuN3 and N719 to ZnO were investigated by monitoring the broad mid-IR absorption signal of injected electrons. They were found to be biphasic, with small, fast (<100 fs), and dominating slow components. The slow components have time constants ranging from a few picoseconds to hundreds of picoseconds, and possibly even longer. Corresponding transient vibrational spectra of these adsorbates and related ReC0A indicate that the appearance of injected electron absorption correlates with the decay of adsorbate excited state. Formation of agglomerates in the sensitized ZnO sample reduces the electron injection quantum yield, but does not significantly affect injection dynamics within 1 ns. Therefore, the slow injection to ZnO is not due to agglomerate formation.

A two-state injection model provides an adequate explanation of the biphasic injection dynamics and the dependence on excitation wavelength. The small fast component is attributed to injection from the unrelaxed excited state above the band edge, while the dominating slow components are assigned to injection from the relaxed excited state near the band edge. Using this model, electron injection to ZnO is estimated to be an order of magnitude slower than to TiO_2. This difference is attributed to the different electronic structures of the conduction bands, which give rise to different conduction band density of states and possible differences in electronic coupling strength to the adsorbate. However, the relative contribution from these factors has yet to be quantified.

Acknowledgment. Financial support was provided by the Division of Chemical Sciences, Office of Basic Energy Research, U.S. Department of Energy. This work is also supported in part by the donors of the Petroleum Research Fund and Emory University Research Committee. T. L. is an Alfred P. Sloan fellow.

References and Notes

(1) Miller, R. J. D.; McLendon, G. L.; Nozik, A. J.; Schmickler, W.; Willig, F. *Surface electron-transfer processes*; VCH publishers, Inc.: New York, 1995.

(2) Kamat, P. V. *Chem. Rev.* **1993**, *93*, 267.

(3) Kamat, P. V. *Prog. React. Kinet.* **1994**, *19*, 277.

(4) Hagfeldt, A.; Gratzel, M. *Chem. Rev.* **1995**, *95*, 49.

(5) O'Regan, B.; Gratzel, M. *Nature* **1991**, *353*, 737.

(6) Bach, U.; Lupo, D.; Comte, P.; Moser, J. E.; Weissortel, F.; Salbeck, J.; Spreitzer, H.; Gratzel, M. *Nature* **1998**, *395*, 583.

(7) Nazeeruddin, M. K.; Kay, A.; Rodicio, I.; Humphrybaker, R.; Muller, E.; Liska, P.; Vlachopoulos, N.; Gratzel, M. *J. Am. Chem. Soc.* **1993**, *115*, 6382.

(8) Asbury, J. B.; Hao, E.; Wang, Y.; Ghosh, H. N.; Lian, T. *J. Phys. Chem. B* **2001**, *105*, 4545.

(9) Asbury, J. B.; Wang, Y.; Lian, T. *J. Phys. Chem. B* **1999**, *103*, 6643.

(10) Bauer, C.; Boschloo, G.; Mukhtar, E.; Hagfeldt, A. *J. Phys. Chem. B* **2001**, *105*, 5585.

(11) Furube, A.; Katoh, R.; Hara, K.; Murata, S.; Arakawa, H.; Tachiya, M. *J. Phys. Chem. B* **2003**, *107*, 4162.

(12) Katoh, R.; Furube, A.; Hara, K.; Murata, S.; Sugihara, H.; Arakawa, H.; Tachiya, M. *J. Phys. Chem. B* **2002**, *106*, 12957.

(13) Benko, G.; Myllyperkio, P.; Pan, J.; Yartsev, A. P.; Sundstrom, V. *J. Am. Chem. Soc.* **2003**, *125*, 1118.

(14) Langdon, B. T.; MacKenzie, V. J.; Asunskis, D. J.; Kelley, D. F. *J. Phys. Chem. B* **1999**, *103*, 11176.

(15) Olsen, C. M.; Waterland, M. R.; Kelley, D. F. *J. Phys. Chem. B* **2002**, *106*, 6211.

(16) Sorantin, P. I.; Scharz, K. *Inorg. Chem.* **1992**, *31*, 567.

(17) Henrich, V.; Cox, P. *The Surface Science of Metal Oxides*; Cambridge University Press: Cambridge, 1996.

(18) Hoffmann, R. *Solids and Surfaces: a chemist's view of bonding in extended structures*; Viley-VCH Inc.: New York, 1988.

(19) Tachibana, Y.; Moser, J. E.; Graetzel, M.; Klug, D. R.; Durrant, J. R. *J. Phys. Chem.* **1996**, *100*, 20056.

(20) Tachibana, Y.; Haque, S. A.; Mercer, I. P.; Durrant, J. R.; Klug, D. R. *J. Phys. Chem. B* **2000**, *104*, 1198.

(21) Tachibana, Y.; Haque, S. A.; Mercer, I. P.; Moser, J. E.; Klug, D. R.; Durrant, J. R. *J. Phys. Chem. B* **2001**, *105*, 7424.

(22) Hannappel, T.; Burfeindt, B.; Storck, W.; Willig, F. *J. Phys. Chem. B* **1997**, *101*, 6799.

(23) Durrant, J. R.; Tachibana, Y.; Mercer, I.; Moser, J. E.; Gratzel, M.; Klug, D. R. *Z. Phys. Chem.* **1999**, *212*, 93.

(24) Heimer, T. A.; Heilweil, E. J.; Bignozzi, C. A.; Meyer, G. J. *J. Phys. Chem. A* **2000**, *104*, 4256.

(25) Heimer, T.; Heilweil, E. J. *J. Phys. Chem. B* **1997**, *101*, 10990.

(26) Kelley, C. A.; Farzad, F.; Thompson, D. W.; Stipkala, J. M.; Meyer, G. J. *Langmuir* **1999**, *15*, 7047.

(27) Ellingson, R. J.; Asbury, J. B.; Ferrere, S.; Ghosh, H. N.; Sprague, J. R.; Lian, T.; Nozik, A. J. *J. Phys. Chem. B* **1998**, *102*, 6455.

(28) Asbury, J. B.; Ellingson, R. J.; Ghosh, H. N.; Ferrere, S.; Nozik, A. J.; Lian, T. *J. Phys. Chem. B* **1999**, *103*, 3110.

(29) Ellingson, R. J.; Asbury, J. B.; Ferrere, S.; Ghosh, H. N.; Sprague, J. R.; Lian, T.; Nozik, A. J. *Z. Phys. Chem. (Muenchen)* **1999**, *212*, 77.

(30) Asbury, J. B.; Wang, Y. Q.; Hao, E. C.; Ghosh, H. N.; Lian, T. *Res. Chem. Intermed.* **2001**, *27*, 315.

(31) Asbury, J. B.; Anderson, N. A.; Hao, E.; Lian, T. *J. Phys. Chem. B* **2003**, *107*, 7376.

(32) Kalloinen, J.; Benko, G.; Sundstrom, V.; Korppi-Tommola, J. E. I.; Yartsev, A. P. *J. Phys. Chem. B* **2002**, *106*, 4396.

(33) Benko, G.; Kalloinen, J.; Korppi-Tommola, J. E. I.; Yartsev, A. P.; Sundstrom, V. *J. Am. Chem. Soc.* **2002**, *124*, 489.

(34) Kuciauskas, D.; Monat, J. E.; Villahermosa, R.; Gray, H. B.; Lewis, N. S.; McCusker, J. K. *J. Phys. Chem. B* **2002**, *106*, 9347.

(35) Meulenkamp, E. *J. Phys. Chem. B* **1998**, *102*, 5566.

(36) Asbury, J. B.; Hao, E.; Wang, Y.; Lian, T. *J. Phys. Chem. B* **2000**, *104*, 11957.

(37) Anderson, N. A.; Ai, X.; Chen, D.; Mohler, D. L.; Lian, T. *J. Phys. Chem. B*, in press.

(38) Wang, Y.; Asbury, J. B.; Lian, T. *J. Phys. Chem. A* **2000**, *104*, 4291.

(39) Ghosh, H. N.; Asbury, J. B.; Weng, Y.; Lian, T. *J. Phys. Chem. B* **1998**, *102*, 10208.

(40) Hao, E.; Anderson, N. A.; Asbury, J. B.; Lian, T. *J. Phys. Chem. B* **2002**, *106*, 10191.

(41) Takeshita, K.; Sasaki, Y.; Kobashi, M.; Tanaka, Y.; Maeda, S.; Yamakata, A.; Ishibashi, T.; Onishi, H. *J. Phys. Chem. B* **2003**, *107*, 4156.

(42) Monat, J. E.; Rodriguez, J. H.; McCusker, J. K. *J. Phys. Chem. A* **2002**, *106*, 7399.

(43) Ghosh, H. N.; Asbury, J. B.; Lian, T. *J. Phys. Chem. B* **1998**, *102*, 6482.

(44) Schoonover, J. R.; Strouse, G. F. *Chem. Rev.* **1998**, *98*, 1335.

(45) Bedja, I.; Kamat, P. V.; Hua, X.; Lappin, A. G.; Hotchandani, S. *Langmuir* **1997**, *13*, 2398.

(46) Sauve, G.; Cass, M. E.; Coia, G.; Doig, S. J.; Lauermann, I.; Pomykal, K. E.; Lewis, N. S. *J. Phys. Chem. B* **2000**, *104*, 6821.

(47) Enright, B.; Fitzmaurice, D. *J. Phys. Chem.* **1996**, *100*, 1027.

(48) Keis, K.; Lindgren, J.; Lindquist, S.-E.; Hagfeldt, A. *Langmuir* **2000**, *16*, 4688.

(49) Horiuchi, H.; Katoh, R.; Hara, K.; Yanagida, M.; Murata, S.; Arakawa, H.; Tachiya, M. *J. Phys. Chem. B* **2003**, *107*, 2570.

(50) Keis, K.; Bauer, C.; Boschloo, G.; Hagfeldt, A.; Westermark, K.; Rensmo, H.; Siegbahn, H. *J. Photochem. Photobio., A: Chem.* **2002**, *148*, 57.

(51) Nazeeruddin, M. K.; Zakeerudin, S. M.; Humphry-Baker, R.; Jirousek, M.; Liska, P.; Vlachopoulos, N.; Shklover, V.; Fischer, C.-H.; Gratzel, M. *Inorg. Chem.* **1999**, *38*, 6298.

(52) Westermark, K.; Rensmo, H.; Siegbahn, H.; Keis, K.; Hagfeldt, A.; Ojamaee, L.; Persson, P. *J. Phys. Chem. B* **2002**, *106*, 10102.

(53) Gao, Y. Q.; Georgievskii, Y.; Marcus, R. A. *J. Chem. Phys.* **2000**, *112*, 3358.

(54) Gao, Y. Q.; Marcus, R. A. *J. Chem. Phys.* **2000**, *113*, 6351.

(55) Redmond, G.; O'Keeffe, A.; Burgess, C.; MacHale, C.; Fitzmaurice, D. *J. Phys. Chem.* **1993**, *97*, 11081.

(56) Petersson, A.; Ratner, M.; Karlsson, H. O. *J. Phys. Chem. B* **2000**, *104*, 8498.

(57) Persson, P.; Lunell, S.; Ojamae, L. *Chem. Phys. Lett.* **2002**, *364*, 469.

(58) Murakoshi, K.; Yanagida, S.; Capel, M.; Castner, J. E. W. Interfacial Electron-Transfer Dynamics of Photosensitized Zinc Oxide Nanoclusters. In *ACS Symposium Series 679*; Shalaev, V. M., Moskovits, M., Eds.; American Chemical Society, Washingtron, DC, 1997; p 221.

(59) Lian, T.; Kitamura, T.; Yanagida, S. Unpublished Result.

(60) Weng, Y.-X.; Wang, Y.-Q.; Asbury, J. B.; Ghosh, H. N.; Lian, T. *J. Phys. Chem. B* **2000**, *104*, 93.

(61) Huber, R.; Sporlein, S.; Moser, J. E.; Gratzel, M.; Wachtveitl, J. *J. Phys. Chem. B* **2000**, *104*, 8995.

(62) Willis, R. L.; Olson, C.; O'Regan, B.; Lutz, T.; Nelson, J.; Durrant, J. R. *J. Phys. Chem. B* **2002**, *106*, 7605.